Available online at www.sciencedirect.com
ScienceDirect
Journal of Sound and Vibration 315 (2008) 1071–1085
JOURNAL OF SOUND AND VIBRATION
www.elsevier.com/locate/jsvi

Vibrations of parallel arrays of electrostatically actuated microplates

Maurizio Porfiri*

Department of Mechanical and Aerospace Engineering, Polytechnic University, Six Metro Tech Center, Brooklyn, NY 11201, USA

Received 30 October 2007; received in revised form 11 January 2008; accepted 6 February 2008
Handling Editor: S. Bolton
Available online 28 March 2008

Abstract

We study small vibrations of a parallel array of microplates predeformed by an electric field. We derive closed-form expressions for the array's modal properties, including resonance frequencies, mode shapes, and modal dampings. Determined expressions depend on the direct current voltage applied across adjacent microplates, on the number of microplates comprising the array, on the boundary conditions imposed on each microplate, and on the geometry and material properties of the array. We also propose a continuum approximation of the array, where the discrete set of microplates' deflections is replaced by a continuous field that represents the envelope of the microplates' displacements. In the continuum approximation, the set of partial differential equations describing the system's dynamics is replaced by a sole partial differential equation. Predictions of the continuum approximation are in very good agreement with the exact solution and provide a new perspective in analyzing complex microsystems.

1. Introduction

Electrostatically actuated microplates are extensively used as microelectromechanical systems (MEMS) in different applications such as signal filtering, chemical sensing, and mass sensing, see for example Refs. [1–4]. An electrostatically actuated microplate is an elastic plate suspended above a stationary rigid plate. Both plates are made of conductive materials, and a dielectric medium fills the gap between them. A direct current (dc) voltage applied across the flexible microplate and the rigid plate deflects the movable microplate towards the rigid plate. A superimposed small alternating current (ac) harmonic voltage forces the flexible microplate to vibrate. The modal properties of the microplate are controlled by the dc voltage. The applied dc voltage has an upper limit beyond which the electrostatic force is not balanced by the elastic restoring force in the deformable microplate, the microplate spontaneously deflects towards the stationary rigid plate, and the MEMS collapses. As the dc voltage increases, the overall system stiffness generally decreases, leading to a drop in the fundamental vibration frequency. The structural instability of electrostatically actuated MEMS due to the gradual increase of electrostatic pressure is usually referred to as the pull-in instability [1–4].

*Tel.: +1 718 260 3681; fax: +1 718 260 3532.
E-mail address: mporfiri@poly.edu

0022-460X/$ - see front matter © 2008 Elsevier Ltd. All rights reserved.
doi:10.1016/j.jsv.2008.02.007

In correspondence to the pull-in instability the fundamental resonance frequency of the MEMS vanishes, see for example Refs. [5,6].

Vibrations and pull-in instability of electrostatically actuated microplates have been extensively studied in the technical literature. Linear elastic microplates are considered in Refs. [5,7]. Empirical reduced-order models for pull-in extraction are presented in Ref. [8]. The significance of membrane stretching on pull-in instability of rectangular and circular microplates are discussed in Refs. [6,9] and Ref. [10], respectively. Vibrations and pull-in instability of microplates of varying cross sections are considered in Ref. [11]. Multilayered microplates are studied in Ref. [12]. The effect of fringing fields on pull-in instability and vibration modes is analyzed in Refs. [13,14]. Pull-in instability analysis of microplates using linear membrane theory is presented in Refs. [15,16]. The influence of Casimir force on pull-in instability of microplates is discussed in Refs. [17–19]. The effect of Van der Waals force on pull-in instability of microplates is studied in Refs. [20,21]. Nonlinear oscillations of microplates due to moderately large applied ac voltages are analyzed in Refs. [22–24]. Accurate analyses of thermoelastic and squeeze-film damping are presented in Refs. [25,26].

Recently, MEMS incorporating arrays of microplates have been proposed for comb-drive actuators [27], chemical detectors [28], resonant microsensors [29], mass sensors [30], tunable filters [31], and cell stiffness measurement systems [32]. MEMS arrays offer great advantages versus single device systems, for their ability to provide distributed sensing and multiple measurements. Pull-in instability of a parallel array of electrostatically actuated microplates is studied in Refs. [33,34]. In Refs. [33,34], numerical results are presented for a lumped system, where the array is modeled as a spring-mass chain, and interactions among adjacent masses are possible through nonlinear springs that lump the surface forces in the array.

In this paper, we analyze vibrations of a parallel array of identical electrostatically actuated microplates. Specifically, we study small oscillations of a parallel array of microplates about static equilibrium configurations determined by a constant dc voltage evenly applied across any two adjacent microplates of the array. We model each element of the array as an arbitrarily shaped thin plate. We derive exact expressions for the resonance frequencies, mode shapes, and modal dampings of the array. We show that as the applied dc voltage increases, the fundamental resonance frequency decreases and eventually vanishes in correspondence to the pull-in instability. We derive an exact expression for the pull-in voltage that is consistent with the numerical findings of Refs. [33,34]. We show that in correspondence to the pull-in instability, the microplates' array deforms in an antisymmetric way, similar to a "saw-tooth" shape. This means that if a microplate is moving upward, the two neighboring ones move downward. The maximum displacement is attained at the midspan of the array. We also present a continuum approximation [35] of the array, where the discrete set of microplates' deflections are replaced by a continuous field. The continuous field represents the envelope of the microplates' displacements. In the continuum approximation, the finite set of partial differential equations governing the vibrations of the microplates' array is replaced by a single partial differential equation for the continuous field. The pull-in instability problem for the continuous model is similar to the classical buckling problem of columns [36]. Predictions of the continuum approximation are in very good agreement with the exact solution and provide a new perspective in analyzing complex microsystems.

The rest of the paper is organized as follows. In Section 2, we describe the MEMS under consideration, and we present the fundamental equations describing small vibrations of the system. In Section 3, we derive exact closed-form expressions for the modal properties of the system, including resonance frequencies, mode shapes, and modal dampings. We also compute the pull-in voltage and analyze the resulting deformations in the array. In Section 4, we illustrate our findings through the analysis of a representative sample problem. In Section 5, we present the continuum approximation and compare its predictions with the exact solution. Section 6 is left for conclusions.

2. Electromechanical model

We consider a parallel array of N identical thin microplates in a dielectric medium of dielectric constant ε, as shown in Fig. 1(a). Microplates are equally spaced by a gap g_0, and have a constant thickness h. Microplates are isotropic and homogeneous. We assume that the microplates are sufficiently close, that is, $g_0 \ll a$, where a is some characteristic microplate dimension, see Fig. 1(b). Each microplate is modelled as a Kirchhoff–Love plate [37], implying that only small deflections are considered. Residual stress, if present, is assumed equal for

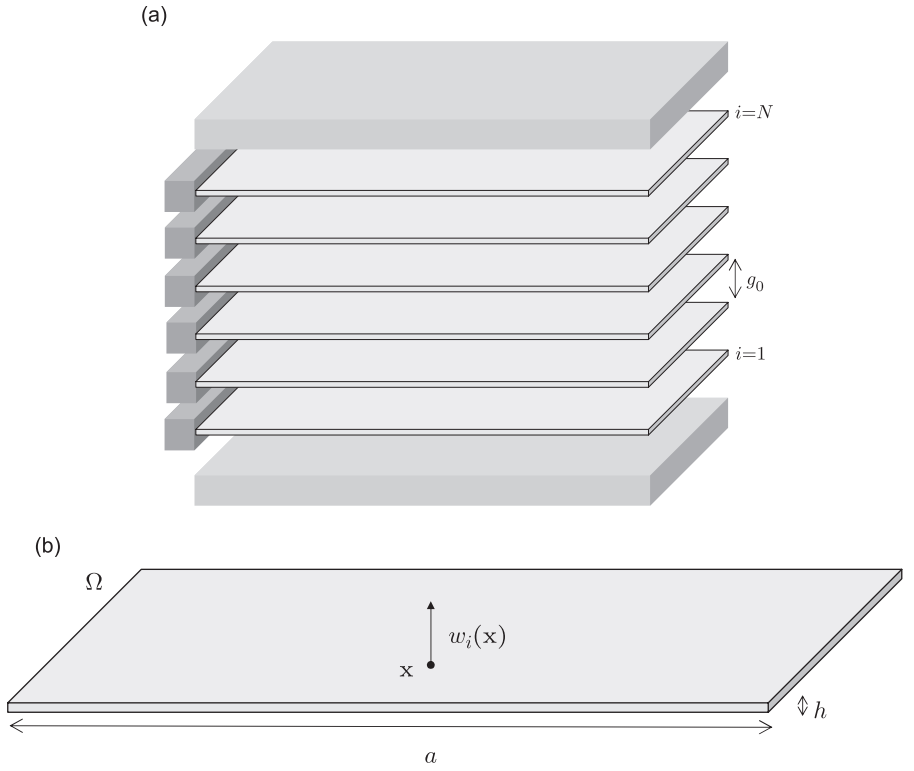

Fig. 1. (a) Sketch of a parallel array of cantilever microplates; (b) sketch of a single microplate illustrating the key variables used in the analysis.

every microplate in the array. We note that rectangular microplates which are free on two opposite edges and are subjected to symmetric loadings can be assimilated to wide microbeams undergoing plane deformations, see for example Ref. [6].

Microplates in the array are labeled through an index i that ranges from 1 to N and increases in the upward direction, as illustrated in Fig. 1(a). The deflection field of the ith microplate is $w_i(\mathbf{x}, t)$, where $\mathbf{x} \in \Omega$ is a common in-plane coordinate for all the microplates and t is the time variable, see Fig. 1(b). The equation of motion for the ith microplate is

$$L[w_i(\mathbf{x}, t)] + \rho h \ddot{w}_i(\mathbf{x}, t) = p_i(\mathbf{x}, t) + c(\dot{w}_{i+1}(\mathbf{x}, t) - 2\dot{w}_i(\mathbf{x}, t) + \dot{w}_{i-1}(\mathbf{x}, t)), \tag{1}$$

where ρ is the microplates' mass per unit volume; c is a coefficient quantifying viscous damping, see for example Ref. [23]; and p_i is the distributed electrostatic load per unit surface area acting on the ith microplate. The linear differential operator L in Eq. (1) is defined by

$$L[w] = B\Delta\Delta w - h\,\mathrm{div}(\sigma\nabla w), \tag{2}$$

where $B = Eh^3/(12(1-\nu^2))$ is the bending stiffness of a microplate; E and ν are the Young's modulus and Poisson's ratio of the material comprising the microplates; σ is the residual in-plane stress tensor; and Δ, div, and ∇ are the Laplace, divergence, and gradient operators, respectively. Boundary conditions need also to be specified to assure that the linear operator L is self-adjoint and positive definite in the space of admissible solutions, see for example Ref. [38]. We consider only homogeneous boundary conditions, and, for ease of illustration, we further assume that the eigenvalues of L are all distinct. We note that through Eq. (2) micromembranes can be considered as microplates of negligible bending stiffness, see for example Ref. [18].

The gap between the ith and the $(i+1)$th microplates at position $\mathbf{x}$ and time t is defined through

$$g_{i,i+1}(\mathbf{x}, t) = g_0 + w_{i+1}(\mathbf{x}, t) - w_i(\mathbf{x}, t). \tag{3}$$

We eliminate edge-effects from our analysis by assuming that two rigid electrodes are present on the bottom and top of the array at a distance g_0 from the first and the last microplate, respectively. The gap between the bottom rigid electrode and the first microplate is

$$g_{0,1}(\mathbf{x},t) = g_0 + w_1(\mathbf{x},t), \tag{4}$$

while the gap between the top rigid electrode and the last microplate is

$$g_{N,N+1}(\mathbf{x},t) = g_0 - w_N(\mathbf{x},t). \tag{5}$$

If the bottom and top rigid electrodes were not present, the following results have to be considered approximately valid for any microplate with the exception of those at the ends of the array, where edge-effects are localized as shown in Ref. [33].

We neglect fringing fields in the array, that is, we assume that every microplate in the array interacts exclusively with the two neighboring microplates. In addition, we use the parallel plate approximation for the electrostatic force, that is, we regard a curved electrode as a superimposition of infinitesimally small parallel plates, see for example Ref. [1]. Within these approximations, the electrostatic load p_i on the ith microplate, at position $\mathbf{x}$ and time t, for $i = 1,\ldots,N$, depends exclusively on the gaps $g_{i,i+1}(\mathbf{x},t)$ and $g_{i-1,i}(\mathbf{x},t)$ in the following way:

$$p_i(\mathbf{x},t) = \frac{\varepsilon V^2}{2}\left(\frac{1}{g_{i,i+1}^2(\mathbf{x},t)} - \frac{1}{g_{i-1,i}^2(\mathbf{x},t)}\right), \tag{6}$$

where V is the dc voltage applied across any pair of adjacent microplates, and the gaps are defined through Eqs. (3)–(5).

The parallel plate approximation is consistent with the linear elastic model of the microplates, and it is accurate for small gaps. For relatively large gaps, more accurate representations can be developed by accounting for the slope and curvature of the microplates [39,40].

We study small vibrations in the neighborhood of the reference configuration, where all the deflection fields w_i's are zero. We note that the reference configuration is an equilibrium configuration, that is, it is a solution of Eq. (1), since it corresponds to vanishing electrostatic loads according to Eq. (6). By linearizing the electrostatic load in Eq. (6) in the neighborhood of the reference configuration, and by using the gap's definition in Eqs. (3)–(5), we obtain the equations of motion for the plates located at the ends of the array

$$L[w_1(\mathbf{x},t)] + \rho h\ddot{w}_1(\mathbf{x},t) = \gamma(-w_2(\mathbf{x},t) + 2w_1(\mathbf{x},t)) + c(\dot{w}_2(\mathbf{x},t) - 2\dot{w}_1(\mathbf{x},t)), \tag{7a}$$

$$L[w_N(\mathbf{x},t)] + \rho h\ddot{w}_N(\mathbf{x},t) = \gamma(2w_N(\mathbf{x},t) - w_{N-1}(\mathbf{x},t)) + c(-2\dot{w}_N(\mathbf{x},t) + \dot{w}_{N-1}(\mathbf{x},t)), \tag{7b}$$

and the equation of motion below for the ith microplate with $i = 2,\ldots,N-1$

$$\begin{aligned} L[w_i(\mathbf{x},t)] + \rho h\ddot{w}_i(\mathbf{x},t) = {} & \gamma(-w_{i+1}(\mathbf{x},t) + 2w_i(\mathbf{x},t) - w_{i-1}(\mathbf{x},t)) \\ & + c(\dot{w}_{i+1}(\mathbf{x},t) - 2\dot{w}_i(\mathbf{x},t) + \dot{w}_{i-1}(\mathbf{x},t)). \end{aligned} \tag{8}$$

In Eqs. (7) and (8), we introduced the positive parameter

$$\gamma = \frac{\varepsilon V^2}{g_0^3}, \tag{9}$$

to quantify the coupling strength between adjacent microplates due to the electrostatic interaction. We note that nonlinear behaviors such as parametric resonances, see for example Ref. [31], cannot be described by the present model due to its linearized characteristics.

By introducing the $N \times N$ matrix $\mathbf{D} = [D_{ij}]$ defined by

$$D_{ij} = \begin{cases} 2 & \text{if } i = j, \\ -1 & \text{if } |i-j| = 1, \\ 0 & \text{otherwise,} \end{cases} \tag{10}$$

Eqs. (7) and (8) can be compactly rewritten as

$$L[w_i(\mathbf{x},t)] + \rho h \ddot{w}_i(\mathbf{x},t) = \sum_{j=1}^{N} D_{ij}(\gamma w_j(\mathbf{x},t) - c\dot{w}_j(\mathbf{x},t)), \quad i = 1,\ldots,N. \tag{11}$$

We note that the matrix $\mathbf{D}$ in Eq. (10) is symmetric and positive definite, and it corresponds to a finite difference scheme of the negative second-order derivative with homogenous boundary conditions, see for example Ref. [41]. We denote with $\{\delta^{(i)}\}_{i=1}^{N}$ the eigenvalues of $\mathbf{D}$ ordered so that $\delta^{(i)} < \delta^{(i+1)}$, for $i = 1,\ldots,N-1$. Following Ref. [41], the ith eigenvalue of $\mathbf{D}$ can be explicitly computed as

$$\delta^{(i)} = 4\sin^2\left(\frac{i\pi}{2(N+1)}\right) \tag{12}$$

and the corresponding eigenvector $\mathbf{v}^{(i)}$ can be compactly written as

$$\mathbf{v}^{(i)} = \left[\sin\left(\frac{i\pi}{N+1}\right), \sin\left(\frac{2i\pi}{N+1}\right), \ldots, \sin\left(\frac{Ni\pi}{N+1}\right)\right]^{\mathsf{T}}, \tag{13}$$

where we used the superscript T for matrix transposition. We use this notation for matrix transposition throughout the manuscript, and we further indicate the jth component of an N dimensional column vector with a subscript j.

We also introduce the mode shapes of an individual microplate. We say that $W_0(\mathbf{x})$ is a mode shape of an individual microplate with resonance radian frequency ω_0, if it satisfies

$$L[W_0(\mathbf{x})] - \omega_0^2 \rho h W_0(\mathbf{x}) = 0, \tag{14}$$

along with the appropriate boundary conditions. We order the resonance radian frequencies $\{\omega_0^{(\alpha)}\}_{\alpha=1}^{\infty}$ and the corresponding mode shapes $\{W_0^{(\alpha)}(\mathbf{x})\}_{\alpha=1}^{\infty}$ to have $\omega_0^{(\alpha)} < \omega_0^{(\alpha+1)}$, for α positive integer. In addition, we normalize the mode shapes to have

$$\rho h \int_{\Omega} W_0^{(\alpha)}(\mathbf{x}) W_0^{(\beta)}(\mathbf{x})\, \mathrm{d}\Omega = \delta_{\alpha\beta}, \tag{15}$$

where $\delta_{\alpha\beta}$ is the Kronecker delta.

3. Modal analysis

In this section, we analyze the modal properties of the microplates' array in terms of the modal properties of an individual microplate and of the coupling strength γ, that measures the electrostatic interaction, see Eq. (9).

3.1. Undamped microplates' array

We say that a column vector function $\mathbf{W}(\mathbf{x})$ is a mode shape of the microplates' array with resonance radian frequency ω, if, for $i = 1,\ldots,N$,

$$L[W_i(\mathbf{x})] - \omega^2 \rho h W_i(\mathbf{x}) = \gamma \sum_{j=1}^{N} D_{ij} W_j(\mathbf{x}), \tag{16}$$

along with the prescribed boundary conditions, that are evenly imposed on each vector element. Eq. (16) is derived from Eq. (11) by discarding viscous damping and by looking for harmonic solutions of Eq. (11).

The components of the vector $\mathbf{W}(\mathbf{x})$ can be expressed in terms of the individual microplate mode shapes $\{W_0^{(\alpha)}(\mathbf{x})\}_{\alpha=1}^{\infty}$ through

$$W_i(\mathbf{x}) = \sum_{\alpha=1}^{\infty} \xi_i^{(\alpha)} W_0^{(\alpha)}(\mathbf{x}), \quad i = 1,\ldots,N, \tag{17}$$

where $\xi_i^{(\alpha)}$ is a real constant. By substituting Eq. (17) into Eq. (16) and by using Eqs. (14) and (15), we find

$$((\omega_0^{(\alpha)})^2 - \omega^2)\xi_i^{(\alpha)} = \frac{\gamma}{\rho h}\sum_{j=1}^{N} D_{ij}\xi_j^{(\alpha)}. \tag{18}$$

We note that Eq. (18) implies that the vector $\boldsymbol{\xi}^{(\alpha)} = [\xi_1^{(\alpha)}, \ldots, \xi_N^{(\alpha)}]^{\mathsf{T}}$ is an eigenvector of the matrix $\mathbf{D}$ with eigenvalue $(\rho h/\gamma)((\omega_0^{(\alpha)})^2 - \omega^2)$.

We use the double index (αi) to identify mode shapes of the array. From Eqs. (13), (17), and (18), we find that the (αi)th mode shape of the microplates' array, say $\mathbf{W}^{(\alpha i)}(\mathbf{x})$, is given by

$$\mathbf{W}^{(\alpha i)}(\mathbf{x}) = W_0^{(\alpha)}(\mathbf{x})\mathbf{v}^{(i)}. \tag{19}$$

Therefore, the (αi)th mode shape of the microplates' array corresponds to the αth mode of vibration of an isolated microplate weighted throughout the array by the eigenvector $\mathbf{v}^{(i)}$.

In addition, from Eq. (12) we find that the corresponding resonance radian frequency $\omega^{(\alpha i)}$ is given by

$$(\omega^{(\alpha i)})^2 = (\omega_0^{(\alpha)})^2 - \frac{\gamma}{\rho h}\delta^{(i)}. \tag{20}$$

We note that if the coupling strength γ is zero, $\omega^{(\alpha i)} = \omega_0^{(\alpha)}$ for every $i = 1, \ldots, N$. That is, the αth resonance frequency of an individual microplate is a resonance frequency for the entire array with multiplicity equal to N. For $\gamma > 0$, the resonance radian frequencies $\{\omega^{(\alpha i)}\}_{i=1}^{N}$ vary and each of them corresponds to a specific mode shape. In particular, microplates' electrostatic interactions introduce a softening effect on the overall system stiffness, since $\omega^{(\alpha N)} < \cdots < \omega^{(\alpha 1)} < \omega_0^{(\alpha)}$. This is consistent with the experimental results of Ref. [31].

3.2. Pull-in instability

The $(1N)$th mode is the fundamental mode of the microplates' array, since it corresponds to the lowest resonance frequency. From Eqs. (12) and (20), the fundamental resonance radian frequency $\omega^{(1N)}$ can be written as

$$\omega^{(1N)} = \sqrt{(\omega_0^{(1)})^2 - \frac{\gamma}{\rho h}\delta^{(N)}} = \sqrt{(\omega_0^{(1)})^2 - 4\frac{\gamma}{\rho h}\sin^2\left(\frac{N\pi}{2(N+1)}\right)}. \tag{21}$$

Moreover, from Eqs. (13) and (19), the fundamental mode shape is

$$\begin{aligned}\mathbf{W}^{(1N)}(\mathbf{x}) &= W_0^{(1)}(\mathbf{x})\mathbf{v}^{(N)} \\ &= W_0^{(1)}(\mathbf{x})\left[\sin\left(\frac{N\pi}{N+1}\right), \sin\left(\frac{2N\pi}{N+1}\right), \ldots, \sin\left(\frac{N^2\pi}{N+1}\right)\right]^{\mathsf{T}}.\end{aligned} \tag{22}$$

Fig. 2(a) shows the dependence of $\delta^{(N)}$ on the array size N. From Fig. 2(a), we evince that $\delta^{(N)}$ is always less than 4 and quickly converges to 4 as N increases. Therefore, as N increases the fundamental radian frequency approaches $\sqrt{(\omega_0^{(1)})^2 - 4(\gamma/(\rho h))}$. Fig. 2(b) shows the vector $\mathbf{v}^{(N)}$ for $N = 20$ and clarifies the behavior of the fundamental mode shape $\mathbf{W}^{(1N)}$. In general, $\mathbf{W}^{(\alpha N)}(\mathbf{x})$ describes a configuration where two adjacent microplates deflect in opposite directions and where microplates located at the midspan of the array deflect more than microplates in the vicinity of the array's ends.

As the coupling strength γ increases, the fundamental resonance frequency in Eq. (21) decreases until it vanishes for the critical coupling strength γ^*, given by

$$\gamma^* = \frac{\rho h(\omega_0^{(1)})^2}{\delta^{(N)}} = \frac{\rho h(\omega_0^{(1)})^2}{4\sin^2(N\pi/(2(N+1)))}. \tag{23}$$

For values of γ lower than the threshold value γ^*, the microplates' array has only one equilibrium configuration corresponding to the reference configuration. This equilibrium configuration is stable, since all the resonance frequencies are positive. As γ approaches the critical value γ^*, the system's overall stiffness

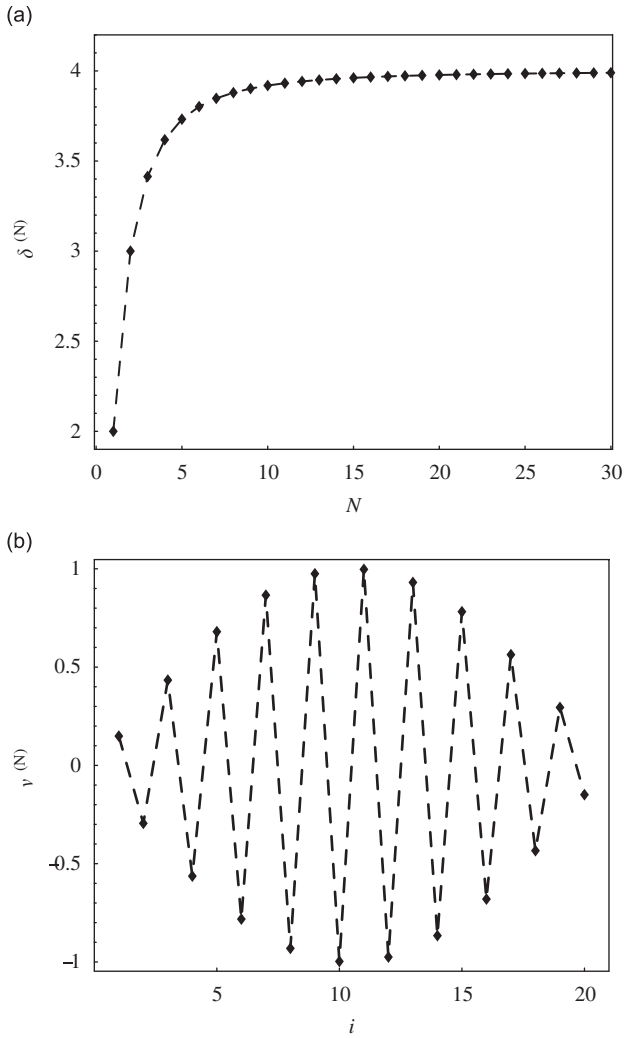

Fig. 2. (a) $\delta^{(N)}$ as a function of N; (b) components of the last eigenvector of $\mathbf{D}$ for $N = 20$.

reduces and vanishes for $\gamma = \gamma^*$. For $\gamma = \gamma^*$, the reference configuration becomes unstable, and a new equilibrium configuration corresponding to the fundamental mode shape, see Eq. (22), arises. The problem is similar to the classical column buckling problem. Eq. (22) states that each microplate deflects along its fundamental mode shape with an amplitude that increases as approaching the array midspan. In addition, adjacent microplates deflect in opposite directions in a "saw-tooth" shape. We also notice that by increasing the size of the array smaller coupling strengths are required to reach the instability, see Eq. (23) and Fig. 2(a).

The pull-in voltage V^* can be derived from Eqs. (9) and (23) as

$$V^* = \omega_0^{(1)} \sqrt{\frac{g_0^3 \rho h}{\varepsilon \delta^{(N)}}} = \omega_0^{(1)} \sqrt{\frac{g_0^3 \rho h}{\varepsilon\, 4\sin^2(N\pi/(2(N+1)))}}. \tag{24}$$

For a large number of microplates, that is, for $N \to \infty$, the pull-in voltage V^* converges to $(\omega_0^{(1)}/2)\sqrt{g_0^3 \rho h/\varepsilon}$. This limit value is consistent with the numerical results derived in Refs. [33,34] for a variety of boundary conditions imposed on individual microplates.

3.3. Damped microplates' array

In this section, we analyze damped vibrations of the microplates' array governed by Eq. (11) using the modal properties determined in Section 3.1. We rewrite the deflection of the ith microplate in terms of the array's mode shapes in Eq. (19) as

$$w_i(\mathbf{x},t)=\sum_{\alpha=1}^{\infty}\sum_{k=1}^{N} q^{(\alpha k)}(t)W_i^{(\alpha k)}(\mathbf{x}), \tag{25}$$

where $\{q^{(\alpha i)}(t)\}_{\alpha=1,i=1}^{\infty,N}$ are the modal coefficients. By replacing Eq. (25) into Eq. (11) and by using Eq. (19), we find

$$\begin{aligned}&\sum_{\alpha=1}^{\infty}\sum_{k=1}^{N} q^{(\alpha i)}(t)L[W_0^{(\alpha)}(\mathbf{x})]v_i^{(k)}+\rho h\sum_{\alpha=1}^{\infty}\sum_{k=1}^{N}\ddot{q}^{(\alpha i)}(t)W_0^{(\alpha)}(\mathbf{x})v_i^{(k)}\\&\quad=\sum_{j=1}^{N}D_{ij}\left(\gamma\sum_{\alpha=1}^{\infty}\sum_{k=1}^{N}q^{(\alpha k)}(t)W_0^{(\alpha)}(\mathbf{x})v_j^{(k)}-c\sum_{\alpha=1}^{\infty}\sum_{k=1}^{N}\dot{q}^{(\alpha k)}(t)W_0^{(\alpha)}(\mathbf{x})v_j^{(k)}\right).\end{aligned} \tag{26}$$

By using the facts that $W_0^{(\alpha)}$ is a mode shape for an individual microplate and that $\mathbf{v}^{(k)}$ is an eigenvector of $\mathbf{D}$, from Eq. (27), we derive

$$\begin{aligned}&\rho h\sum_{\alpha=1}^{\infty}\sum_{k=1}^{N}(\ddot{q}^{(\alpha i)}(t)+(\omega_0^{(\alpha)})^2q^{(\alpha i)}(t))W_0^{(\alpha)}(\mathbf{x})v_i^{(k)}\\&\quad=\gamma\sum_{\alpha=1}^{\infty}\sum_{k=1}^{N}q^{(\alpha k)}(t)W_0^{(\alpha)}(\mathbf{x})\delta^{(k)}v_i^{(k)}-c\sum_{\alpha=1}^{\infty}\sum_{k=1}^{N}\dot{q}^{(\alpha k)}(t)W_0^{(\alpha)}(\mathbf{x})\delta^{(k)}v_i^{(k)}.\end{aligned} \tag{27}$$

By exploiting the orthogonality of the mode shapes $W_0^{(\alpha)}$ and of the eigenvectors $\mathbf{v}^{(k)}$, from Eqs. (20) and (27), we conclude that

$$\ddot{q}^{(\alpha i)}(t)+(\omega^{(\alpha i)})^2q^{(\alpha i)}(t)+\frac{c\delta^{(i)}}{\rho h}\dot{q}^{(\alpha i)}(t)=0. \tag{28}$$

The modal damping for the (αi)th mode can be computed from Eq. (28) as

$$\zeta^{(\alpha i)}=\frac{c\delta^{(i)}}{2\omega^{(\alpha i)}\rho h}. \tag{29}$$

As the coupling strength γ increases the modal damping $\zeta^{(\alpha i)}$ increases. In particular, even for small viscous damping, the fundamental vibration mode can be made over-damped by increasing the coupling strength γ, that is by increasing the dc voltage V.

4. Sample problem

We consider an array of $N=20$ rectangular cantilever microplates of dimensions $a\times b$, with $a\gg b$, and we further assume that the residual stress is zero. The first five resonance frequencies of an individual microplate are reported in Table 1.

The resonance radian frequencies of the microplates' array are given by Eq. (20), that can be rearranged into

$$\frac{\omega^{(\alpha i)}}{\omega_0^{(1)}}=\sqrt{\frac{(\omega_0^{(\alpha)})^2}{(\omega_0^{(1)})^2}-\tilde{\gamma}\delta^{(i)}}, \tag{30}$$

where we defined the nondimensional coupling strength $\tilde{\gamma}=\gamma/(\rho h(\omega_0^{(1)})^2)$. We recall that the parameters $\delta^{(i)}$'s are defined in Eq. (12). The modal damping of the (αi)th mode of the microplates' array in Eq. (29) can be

Table 1
Natural radian frequency of an individual microplate

	$\alpha = 1$	$\alpha = 2$	$\alpha = 3$	$\alpha = 4$	$\alpha = 5$
$\sqrt{\omega_0}a\sqrt[4]{\frac{\rho h}{B}}$	1.875104	4.694091	7.854757	10.995540	14.137168

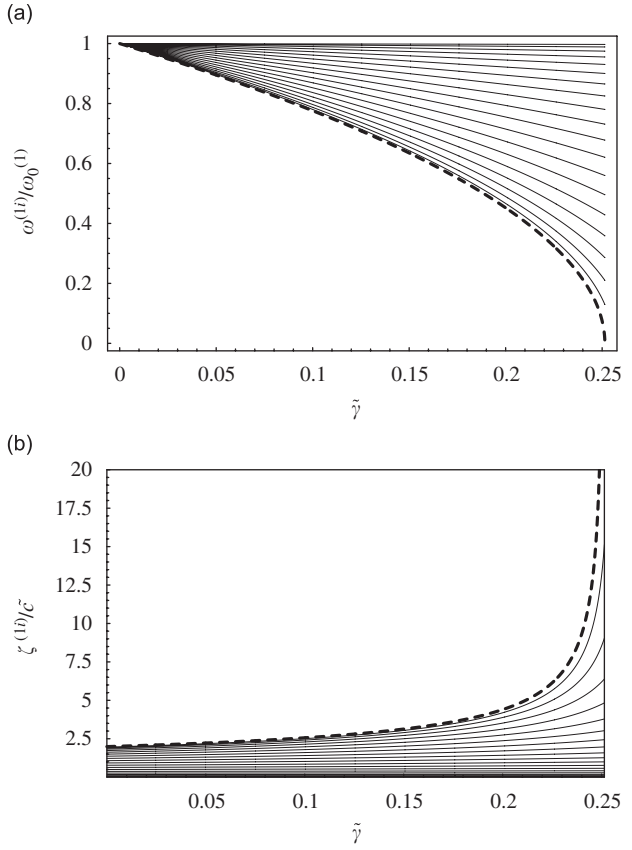

Fig. 3. (a) $\omega^{(1i)}/\omega_0^{(1)}$ as a function of $\tilde{\gamma}$, dashed line refers to the fundamental mode; (b) $\zeta^{(1i)}/\tilde{c}$ as a function of $\tilde{\gamma}$, dashed line refers to the fundamental mode.

rewritten as

$$\zeta^{(\alpha i)} = \tilde{c}\frac{\delta^{(i)}\omega_0^{(1)}}{2\omega^{(\alpha i)}}, \tag{31}$$

where we defined the nondimensional viscous damping $\tilde{c} = c/(\rho h\omega_0^{(1)})$.

In Fig. 3(a), we report the nondimensional resonance radian frequencies $\omega^{(1i)}/\omega_0^{(1)}$ defined in Eq. (30) in terms of the nondimensional coupling strength $\tilde{\gamma}$. In Fig. 3(b), we report the scaled modal dampings $\zeta^{(1i)}/\tilde{c}$ defined in Eq. (31) in terms of the nondimensional coupling strength $\tilde{\gamma}$. From Fig. 3(a), we note that as $\tilde{\gamma}$ increases the fundamental resonance frequency decreases until it vanishes for $\tilde{\gamma} = 0.2514$. In correspondence of $\tilde{\gamma} = 0.2514$, a new equilibrium configuration corresponding to the fundamental mode shape, see Eq. (22), arises. In Fig. 4, we report the critical deflection profile resulting at the pull-in instability, that is computed according to Eq. (22). In Fig. 5(a), we report the first five nondimensional resonance frequencies $\omega^{(\alpha i)}/\omega_0^{(1)}$ computed from Eq. (30) in terms of the nondimensional coupling strength $\tilde{\gamma}$. In Fig. 5(b), we report the first

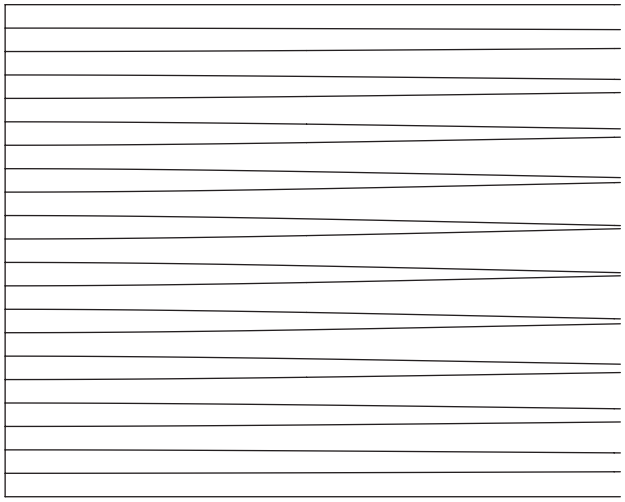

Fig. 4. Front view of critical deflection for the array of cantilever microplates.

five scaled modal damping $\zeta^{(\alpha i)}/\tilde{c}$ computed from Eq. (31) in terms of the nondimensional coupling strength $\tilde{\gamma}$. Fig. 5(a) shows that as the parameter $\tilde{\gamma}$ increases, the ordering of the radian frequencies $\omega^{(\alpha i)}$ changes. Therefore, all the modal properties of the microplates' array, including resonance frequencies, mode shapes, and modal dampings, can be tuned by properly controlling the coupling strength γ, that is, through a fine adjustment of the dc voltage applied across adjacent microplates.

5. Approximate solution through continuum modeling

For a relatively large number of microplates in the array, we can describe the electromechanical system using a continuum approximation. Within this framework, the system of linear partial differential equations in Eq. (11) can be replaced with a single linear partial differential equation. The continuum approximation is valid if the envelope of microplates' deflections is smooth. Continuum approximations have been extensively used to study oscillations of periodic chains of linear [42,43] and nonlinear oscillators [44–47].

Motivated by the discrete analysis conducted above, see for example Eqs. (13) and (19) and Figs. 2(b) and 4, we look for mode shapes such that the microplates' array predominantly deflects in a "saw-tooth" form. To this aim, we introduce the staggered transformation $u_i(\mathbf{x},t) = (-1)^i w_i(\mathbf{x},t)$, see for example Ref. [47], through which Eq. (11) becomes

$$L[u_i(\mathbf{x},t)] + \rho h \ddot{u}_i(\mathbf{x},t) = 4\gamma u_i(\mathbf{x},t) - 4c\dot{u}_i(\mathbf{x},t) - \sum_{i=1}^{N} D_{ij}(\gamma u_j(\mathbf{x},t) - c\dot{u}_j(\mathbf{x},t)), \quad i = 1,\ldots,N, \tag{32}$$

where $u_0(\mathbf{x})$ and $u_{N+1}(\mathbf{x})$ are the vanishing staggered displacements of the bottom and top electrodes, respectively.

We define a vertical abscissa z along the direction of the microplates' deflection. The interspacing between the mid-surfaces of adjacent microplates is $\varepsilon = g_0 + h$. The vertical extension of the array, including the bottom and top rigid electrodes, is $L = (N+1)\varepsilon$. The midsurface of the ith microplate is identified by $z = i\varepsilon$. The staggered displacements can be viewed as discrete samples of a continuous function of the abscissa z, that we call $u(\mathbf{x},z,t)$, that is, $u_i(\mathbf{x},t) = u(\mathbf{x},z,t)$. In addition, by assuming that the staggered displacement field is a smooth function of the vertical abscissa z, $u_{i\pm1}(\mathbf{x},t)$ can be expressed using a McLaurin expansion as

$$u_{i\pm1}(\mathbf{x},t) = u(\mathbf{x},z\pm\varepsilon,t) = u(\mathbf{x},z,t) \pm \varepsilon\frac{\partial u(\mathbf{x},z,t)}{\partial z} + \frac{\varepsilon^2}{2}\frac{\partial^2 u(\mathbf{x},z,t)}{\partial z^2} + \cdots . \tag{33}$$

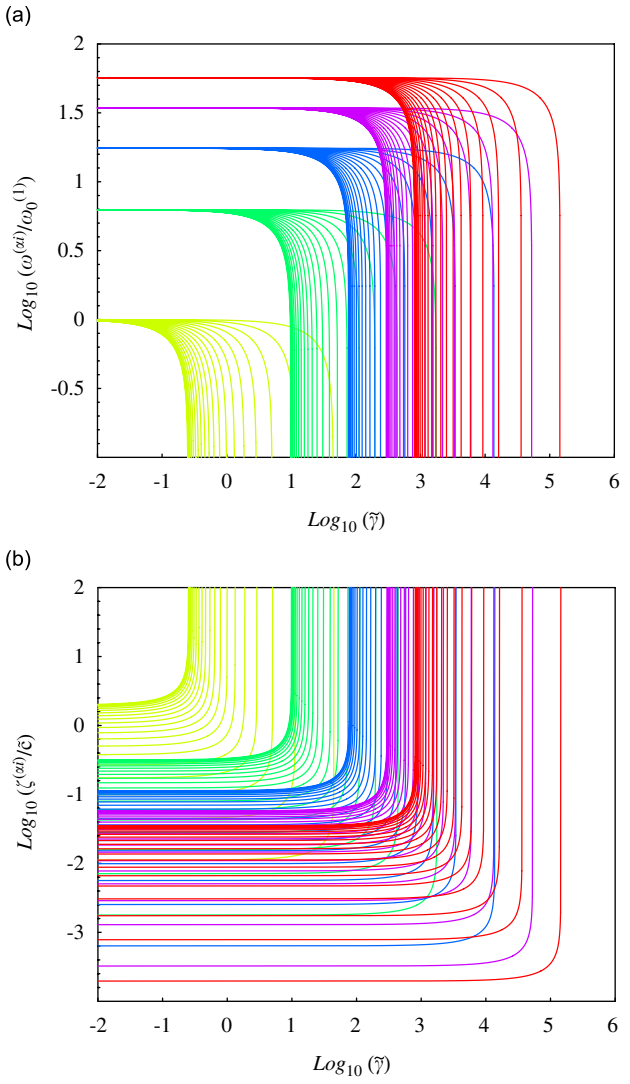

Fig. 5. (a) $\omega^{(\alpha i)}/\omega_0^{(1)}$ as a function of $\tilde{\gamma}$, (b) $\zeta^{(\alpha i)}/\tilde{c}$ as a function of $\tilde{\gamma}$. Yellow curves refer to mode shapes (1i), green curves refer to mode shapes (2i), blue curves refer to mode shapes (3i), purple curves refer to mode shapes (4i), and red curves refer to mode shapes (5i). (For interpretation of the references to color in this figure legend, the reader is referred to the web version of this article).

Eq. (33) can be formally rewritten using the pseudo-differential operator $\exp(\pm\varepsilon(\partial/\partial z))$ as

$$u_{i\pm1}(\mathbf{x},t) = \exp\left(\pm\varepsilon\frac{\partial}{\partial z}\right)[u(\mathbf{x},z,t)]. \tag{34}$$

Therefore, by accounting for the definition of $\mathbf{D}$ in Eq. (10), Eq. (32) can be replaced by the following equation that is valid for $z \in (0, L)$:

$$L[u(\mathbf{x},z,t)] + \rho h\ddot{u}(\mathbf{x},z,t) = 4\gamma u(\mathbf{x},z,t) - 4c\dot{u}(\mathbf{x},z,t) + \mathscr{D}[\gamma u(\mathbf{x},z,t) - c\dot{u}(\mathbf{x},z,t)]. \tag{35}$$

Here, we introduced the pseudo-differential operator $\mathscr{D}$ defined by

$$\mathscr{D} = -4\sin^2\left(\frac{\mathrm{I}\varepsilon}{2}\frac{\partial}{\partial z}\right), \tag{36}$$

where I is the imaginary unit.

Different continuous models for the electrostatically actuated array of microplates can be obtained by properly approximating the pseudo-differential operator in Eq. (36). Using the McLaurin expansion suggested in Ref. [43], we can express $\mathscr{D}$ as

$$\mathscr{D} = \varepsilon^2 \frac{\partial^2}{\partial z^2} + \frac{\varepsilon^4}{12}\frac{\partial^4}{\partial z^4} + \frac{\varepsilon^6}{360}\frac{\partial^6}{\partial z^6} \cdots . \tag{37}$$

Therefore, we find the following general form for a class of continuous models

$$L[u(\mathbf{x},z,t)] + \rho h \ddot{u}(\mathbf{x},z,t) = 4\gamma u(\mathbf{x},z,t) - 4c\dot{u}(\mathbf{x},z,t) + \mathscr{D}_{\mathfrak{o}}[\gamma u(\mathbf{x},z,t) - c\dot{u}(\mathbf{x},z,t)], \tag{38}$$

where $\mathscr{D}_{\mathfrak{o}}$ is a differential operator of order $2\mathfrak{o}$ constructed by retaining the first $\mathfrak{o}$ summands in Eq. (37), with $\mathfrak{o}$ positive integer. Following Ref. [43], we impose homogenous boundary conditions at $z = 0$ and L of the form

$$\frac{\partial^{2d}}{\partial z^{2d}} u(\mathbf{x},0,t) = \frac{\partial^{2d}}{\partial z^{2d}} u(\mathbf{x},L,t), \quad d = 0,\ldots,\mathfrak{o}. \tag{39}$$

We note that alternative continuous models can be derived by using one or two-points Pade's approximations of $\mathscr{D}$, as discussed in Ref. [43].

We say that a function $U(\mathbf{x},z)$ is a mode shape for the continuous model in Eq. (38) with radian resonance frequency $\overline{\omega}$, if it satisfies the following equation:

$$L[U(\mathbf{x},z)] - \overline{\omega}^2 \rho h U(\mathbf{x},z) - 4\gamma U(\mathbf{x},z) - \gamma \mathscr{D}_{\mathfrak{o}}[U(\mathbf{x},z)] = 0, \tag{40}$$

along with the proper boundary conditions. Eq. (40) is obtained from Eq. (38) by discarding the viscous damping c and by looking for harmonic solutions of Eq. (38). By using the separation of variables, the mode shapes can be expressed as the product between the mode shapes of an individual microplate in Eq. (14) and the eigenfunctions of the differential operator $-\mathscr{D}_{\mathfrak{o}}$ with the boundary conditions in Eq. (39). The eigenvalues $\{\lambda^{(\beta)}\}_{\beta=1}^{\infty}$ and the corresponding eigenfunctions $\{v^{(\beta)}(z)\}_{\beta=1}^{\infty}$ of $-\mathscr{D}_{\mathfrak{o}}$ can be expressed as

$$\lambda^{(\beta)} = \varepsilon^2 \left(\frac{\beta\pi}{L}\right)^2 - \varepsilon^4 \frac{1}{12}\left(\frac{\beta\pi}{L}\right)^4 + \varepsilon^6 \frac{1}{360}\left(\frac{\beta\pi}{L}\right)^6 + \cdots + \mathrm{o}(\varepsilon^{2\mathfrak{o}}). \tag{41a}$$

$$v^{(\beta)}(z) = \sqrt{\frac{2}{L}} \sin\left(\beta \frac{\pi z}{L}\right), \tag{41b}$$

Therefore, the $(\alpha\beta)$th mode shape of the continuum approximation can be written as

$$U^{(\alpha\beta)}(\mathbf{x},z) = W_0^{(\alpha)}(\mathbf{x}) v^{(\beta)}(z), \tag{42}$$

where $W_0^{(\alpha)}(\mathbf{x})$ is defined in Eq. (14) and $v^{(\beta)}(z)$ is defined in Eq. (41b). By substituting Eq. (42) into Eq. (40), we determine the resonance radian frequencies of the microplates' array within the continuum approximation

$$\overline{\omega}^{(\alpha\beta)} = \sqrt{(\omega_0^{(\alpha)})^2 - \frac{\gamma}{\rho h}(4 - \lambda^{(\beta)})}. \tag{43}$$

Since the continuum approximation describes a finite array of N microplates, only the values of β ranging from 1 to N are physically admissible. With this in mind, $\lambda^{(\beta)}$ defined in Eq. (41b) is positive and the fundamental resonance radian frequency is $\overline{\omega}^{(11)}$. The critical coupling strength is determined by setting $\overline{\omega}^{(11)} = 0$, that is,

$$\gamma^*_{\mathrm{cont}} = \frac{\rho h (\omega_0^{(\alpha)})^2}{4 - \lambda^{(1)}}, \tag{44}$$

where we used the subscript "cont" to clearly refer to continuum modeling. Consequently, the critical deflection corresponds to the lowest structural mode $U^{(11)}$. Comparing the critical deflection computed in the discrete case and the critical deflection derived in the continuum limit, we note that they yield the same result.

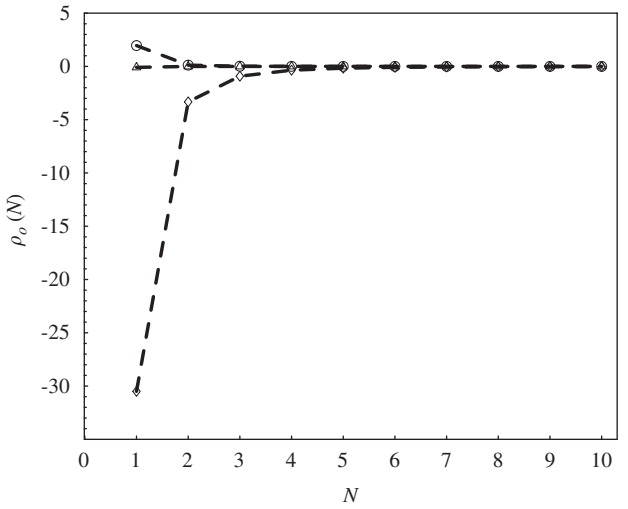

Fig. 6. Percentile error of different continuum models computed using Eq. (45). Diamonds refer to $\mathfrak{o} = 1$, circles refer to $\mathfrak{o} = 2$, and triangles refer to $\mathfrak{o} = 3$.

On the other hand, we note that the critical values of γ, reported in Eqs. (23) and (14), are equal only in the limit of $N \to \infty$. In order to quantify the error in the estimation of the critical coupling strength of the continuum model of order $\mathfrak{o}$, we introduce the quantity $\rho_{\mathfrak{o}}(N)$ defined as

$$\rho_{\mathfrak{o}}(N) = 100\frac{\gamma^* - \gamma^*_{\text{cont}}}{\gamma^*}. \tag{45}$$

The function $\rho_{\mathfrak{o}}(N)$ is plotted in Fig. 6 for $\mathfrak{o} = 1, 2, 3$. We note that as the order of the truncation $\mathfrak{o}$ increases, the accuracy of the continuum model improves. For $\mathfrak{o} = 3$, the predictions of the continuum model are barely distinguishable from the exact solution. This indicates that for a limited number of microplates, high-order approximations of the pseudo-differential operator $\mathscr{D}$ defined in Eq. (36) are needed. On the other hand, for a considerably large number of microplates, low-order approximations of $\mathscr{D}$ are sufficient to accurately describe electrostatic coupling in the continuum approximation.

6. Conclusions

We investigated small vibrations of a parallel array of identical microplates predeformed by an electric field. We derived closed-form expressions for the modal properties and pull-in instability of the array. We showed that the modal properties of the array, including resonance frequencies and modal dampings can be adjusted by changing the coupling among the microplates. That is, the vibrational properties of the array can be tuned by properly selecting the dc voltage applied across adjacent microplates.

We also proposed a new continuum approximation to accurately describe the microplates' array. In this framework the array is regarded as a continuous medium and a single displacement field is used to describe the configuration of the array. A single partial differential equation is sufficient to study vibrations and pull-in instability. The continuum approximation is validated using the exact solution.

Acknowledgments

The author sincerely thanks the anonymous reviewers for careful reading of the manuscript and for giving useful suggestions that have helped improve the work and its presentation.

References

[1] J.A. Pelesko, D.H. Bernstein, *Modeling MEMS and NEMS*, Chapman & Hall, Boca Raton, FL, 2002 (Chapter 7).

[2] A. Fargas Marquès, R. Costa Castelló, A.M. Shkel, Modelling the electrostatic actuation of MEMS: state of the art 2005, Technical Report 2005. ⟨URL http://bibliotecnica.upc.es/reports/ioc/IOC-DT-P-2005-18.pdf⟩.

[3] R.M. Lin, W.J. Wang, Structural dynamics of microsystems—current state of research and future directions, *Mechanical Systems and Signal Processing* 20 (5) (2006) 1015–1043.

[4] R.C. Batra, M. Porfiri, D. Spinello, Review of modeling electrostatically actuated microelectromechanical systems, *Smart Materials and Structures* 16 (6) (2007) R23–R31.

[5] H.A. Tilmans, R. Legtenberg, Electrostatically driven vacuum-encapsulated polysilicon resonators: part I. Design and fabrication, *Sensors and Actuators A* 45 (1) (1994) 57–66.

[6] E.M. Abdel-Rahman, M.I. Younis, A.H. Nayfeh, Characterization of the mechanical behavior of an electrically actuated microbeam, *Journal of Micromechanics and Microengineering* 12 (6) (2002) 759–766.

[7] P.C.-P. Chao, C.-W. Chiu, C.-Y. Tsai, A novel method to predict the pull-in voltage in a closed form for micro-plates actuated by a distributed electrostatic force, *Journal of Micromechanics and Microengineering* 16 (5) (2006) 986–998.

[8] S. Pamidighantam, R. Puers, K. Baert, H.A.C. Tilmans, Pull-in voltage analysis of electrostatically actuated beam structures with fixed–fixed and fixed–free end conditions, *Journal of Micromechanics and Microengineering* 12 (4) (2002) 458–464.

[9] X. Zhao, E.M. Abdel-Rahman, A.H. Nayfeh, A reduced-order model for electrically actuated microplates, *Journal of Micromechanics and Microengineering* 14 (7) (2004) 900–906.

[10] G.W. Vogl, A.H. Nayfeh, A reduced-order model for electrically actuated clamped circular plates, *Journal of Micromechanics and Microengineering* 15 (4) (2005) 684–690.

[11] J.-H. Kuang, C.-J. Chen, Dynamic characteristics of shaped micro-actuators solved using the differential quadrature method, *Journal of Micromechanics and Microengineering* 14 (4) (2004) 647–655.

[12] G. Rezazadeh, A comprehensive model to study nonlinear behavior of multilayered micro beam switches, *Microsystem Technologies* accepted for publication, doi:10.1007/s00542-007-0398-x.

[13] R.C. Batra, M. Porfiri, D. Spinello, Electromechanical model of electrically actuated narrow microbeams, *Journal of Microelectromechanical Systems* 15 (5) (2006) 1175–1189.

[14] R.C. Batra, M. Porfiri, D. Spinello, Vibrations of narrow microbeams predeformed by an electric field, *Journal of Sound and Vibration* 309 (3) (2008) 600–612.

[15] J.A. Pelesko, X.Y. Chen, Electrostatic deflections of circular elastic membranes, *Journal of Electrostatics* 57 (1) (2003) 1–12.

[16] R.C. Batra, M. Porfiri, D. Spinello, Analysis of electrostatic MEMS using meshless local Petrov-Galerkin (MLPG) method, *Engineering Analysis with Boundary Elements* 30 (11) (2006) 949–962.

[17] R.C. Batra, M. Porfiri, D. Spinello, Effects of Casimir force on pull-in instability in micromembranes, *Europhysics Letters* 77 (2) (2007) 20010.

[18] R.C. Batra, M. Porfiri, D. Spinello, Reduced-order models for microelectromechanical rectangular and circular plates incorporating the Casimir force, *International Journal of Solids and Structures* (2008), doi:10.1016/j.ijsolstr.2008.02.019.

[19] R.C. Batra, M. Porfiri, D. Spinello, Vibrations and pull-in instabilities of microelectromechanical von Karman elliptic plates incorporating the Casimir force, *Journal of Sound and Vibration* (2008), doi:10.1016/j.jsv.2008.02.008.

[20] A. Ramezani, A. Alasty, J. Akbari, Influence of van der Waals force on the pull-in parameters of cantilever type nanoscale electrostatic actuators, *Microsystem Technologies* 12 (12) (2006) 1153–1161.

[21] R.C. Batra, M. Porfiri, D. Spinello, Effects of van der Waals force and thermal stress on pull-in instability of microplates, *Sensors* 8 (2008) 1048–1069.

[22] A.H. Nayfeh, M.I. Younis, Dynamics of MEMS resonators under superharmonic and subharmonic excitations, *Journal of Micromechanics and Microengineering* 15 (2005) 1840–1847.

[23] M.I. Younis, A.H. Nayfeh, A study of the nonlinear response of a resonant microbeam to an electric actuation, *Nonlinear Dynamics* 31 (1) (2003) 91–117.

[24] W.C. Xie, H.P. Lee, S.P. Lim, Nonlinear dynamic analysis of MEMS switches by nonlinear modal analysis, *Nonlinear Dynamics* 31 (3) (2003) 243–256.

[25] A.H. Nayfeh, M.I. Younis, Modeling and simulations of thermoelastic damping in microplates, *Journal of Micromechanics and Microengineering* 14 (2004) 1711–1717.

[26] V. Ostasevicius, R. Dauksevicius, R. Gaidys, A. Palevicius, Numerical analysis of fluid–structure interaction effects on vibrations of cantilever microstructure, *Journal of Sound and Vibration* 308 (3–5) (2007) 660–673.

[27] G. Zhou, P. Dowd, Tilted folded-beam suspension for extending the stable travel range of comb-drive actuators, *Journal of Micromechanics and Microengineering* 13 (2) (2003) 178–183.

[28] H.P. Lang, M. Hegner, C. Gerber, Cantilever array sensors, *Materials Today* 8 (4) (2005) 30–36.

[29] B.E. De Martini, J.F. Rhoads, S.W. Shaw, K.L. Turner, Single input-single output mass sensor based on a coupled array of microresonators, *Sensors and Actuators A* 137 (1) (2007) 147–156.

[30] M. Spletzer, A. Raman, A.Q. Wu, X. Xu, R. Reifenberger, Ultrasensitive mass sensing using mode localization in coupled microcantilevers, *Applied Physics Letters* 88 (2006) 254102.

[31] E. Buks, M.L. Roukes, Electrically tunable collective response in a coupled micromechanical array, *Journal of Microelectromechanical Systems* 11 (6) (2002) 802–807.

[32] F.M. Sasoglu, A.J. Bohl, B.E. Layton, Design and microfabrication of a high-aspect-ratio pdms microbeam array for parallel nanonewton force measurement and protein printing, *Journal of Micromechanics and Microengineering* 17 (3) (2007) 623–632.
[33] J. Zhu, C.Q. Ru, A. Mioduchowski, Structural instability of a parallel array of mutually attracting identical microbeams, *Journal of Micromechanics and Microengineering* 16 (10) (2006) 2220–2229.
[34] J. Zhu, C.Q. Ru, A. Mioduchowski, Instability of a large coupled microbeam array initialized at its two ends, *The Journal of Adhesion* 83 (3) (2007) 195–221.
[35] A.M. Kosevich, *The Crystal Lattice: Phonons, Solitons, Dislocations, Superlattices*, second ed., Wiley-Vch, Weinheim, Germany, 2005.
[36] S.S. Antman, *Nonlinear Problems of Elasticity*, second ed., Applied Mathematical Sciences, Springer, New York, USA, 2004.
[37] S. Timoshenko, J.N. Goodier, *Theory of Elasticity*, third ed., McGraw-Hill, New York, USA, 1970.
[38] B.D. Reddy, *Introductory Functional Analysis with Applications to Boundary Value Problems and Finite Elements*, Springer, New York, USA, 1998.
[39] J.A. Pelesko, T.A. Driscoll, The effect of the small-aspect-ratio approximation on canonical electrostatic MEMS models, *Journal of Engineering Mathematics* 53 (3–4) (2005) 239–252.
[40] S. Krylov, S. Seretensky, Higher order correction of electrostatic pressure and its influence on the pull-in behavior of microstructures, *Journal of Micromechanics and Microengineering* 16 (7) (2006) 1382–1396.
[41] A. Samarskii, E. Nikolaev, *Numerical Methods for Grid Equations*, Birkhauser Verlag, Basel, Switzerland, 1989.
[42] I.V. Andrianov, J. Awrejcewicz, On the average continuous representation of an elastic discrete medium, *Journal of Sound and Vibration* 264 (5) (2003) 1187–1194.
[43] I.V. Andrianov, J. Awrejcewicz, Continuous models for 1D discrete media valid for higher-frequency domain, *Physics Letters A* 345 (1–3) (2005) 55–62.
[44] P. Rosenau, Quasi-continuous spatial motion of a mass-spring chain, *Physica D* 27 (1–2) (1987) 224–234.
[45] M. Sayadi, J. Pouget, Soliton dynamics in a microstructured lattice model, *Journal of Physics A* 24 (9) (1991) 2151–2172.
[46] A.F. Vakakis, M.E. King, A.J. Pearlstein, Forced localization in a periodic chain of nonlinear oscillators, *International Journal of Nonlinear Mechanics* 29 (3) (1994) 429–447.
[47] B.-F. Feng, D. Yusuke, T. Kawahara, A regularized model equation for discrete breathers in anharmonic lattices with symmetric nearest-neighbor potentials, *Physica D: Nonlinear Phenomena* 214 (1) (2006) 33–41.